# Contrasting Impacts of Two Types of ENSO on the Boreal Spring Hadley Circulation

JUAN FENG AND JIANPING LI

*State Key Laboratory of Numerical Modeling for Atmospheric Sciences and Geophysical Fluid Dynamics, Institute of Atmospheric Physics, Chinese Academy of Sciences, Beijing, China*

(Manuscript received 16 May 2012, in final form 23 December 2012)

ABSTRACT

The possible influences of two types of ENSO [i.e., the canonical ENSO and ENSO Modoki (EM)] on Hadley circulation (HC) during the boreal spring are investigated during 1979–2010. El Niño events are featured with a symmetric pattern in equatorial zonal-mean sea surface temperature anomalies (SSTA), with a maximum around the equator. In contrast, the zonal-mean SSTA associated with El Niño Modoki events shows an asymmetric structure with a maximum around 10°N. The contrasting underlying thermal structures corresponding with ENSO and EM have opposite impacts on the simultaneous HC. In El Niño years, a symmetric anomalous meridional circulation is seen, with enhanced rising around the equator and anomalous descent at about 15°N and 20°S. In contrast, an asymmetric equatorial meridional circulation is observed for El Niño Modoki years, with anomalous ascent around 10°N and descent at about 10°S and 20°N. The contrasting meridional circulation anomalies within ENSO and EM are caused by their different meridional SSTA structure. This result is theoretically explained, indicating that anomalous meridional circulation is subject to the meridional SSTA gradient. Moreover, the observed results are reproduced in numerical experiments driven by anomalous warming in the eastern and central Pacific Ocean. Thus, the authors conclude that the anomalous HC linked to ENSO and EM is induced by the accompanying meridional gradient in zonal-mean SSTA.

## 1. Introduction

The Hadley circulation (HC) is the largest and one of the most important atmospheric circulation systems on the planet and is defined as the zonal-mean meridional mass circulation in the atmosphere bounded roughly by 30°S and 30°N. The HC is a thermally driven meridional circulation with warmer air rising in the tropics and cooler air sinking in the subtropics (Held and Hou 1980). It is characterized by equatorward mass transport by the prevailing trade winds in the lower troposphere and poleward mass transport in the upper troposphere (Quan et al. 2004). The HC is fundamentally important to the global climate and plays an essential role in influencing the climate at low, middle, and high latitudes (e.g., Lindzen 1994; Chang 1995; Hou 1998; Diaz and Bradley 2004).

*Corresponding author address:* Dr. Jianping Li, Deputy Director and Professor, State Key Laboratory of Numerical Modeling for Atmospheric Sciences and Geophysical Fluid Dynamics, Institute of Atmospheric Physics, Chinese Academy of Sciences, 40 HuaYan Li, ChaoYang District, Beijing 100029, China.
E-mail: ljp@lasg.iap.ac.cn

DOI: 10.1175/JCLI-D-12-00298.1



Given that the HC is a thermally driven circulation, it is strongly influenced by the underlying thermal structure in the tropics. El Niño–Southern Oscillation (ENSO) is the most prominent mode of interannual variability in the earth's climate system and has a marked impact on global climate. The influences of ENSO on HC have been intensely addressed. For example, observational and diagnostic analyses have shown that during an El Niño event the tropical atmosphere warms at all longitudes and the subtropical jets in both hemispheres strengthen on their equatorial flanks, indicating an intensified HC (Seager et al. 2003). Quan et al. (2004) reported that a strengthening of HC during the boreal winter [December–February (DJF)] is associated with a warming trend in the tropical oceans and an increased El Niño frequency since 1976. However, this was questioned in Mitas and Clement (2005), in which they indicated that the upward trend of HC cannot be attributed to increasing ENSO frequency. Subsequently, studies by Ma and Li (2007, 2008) and Feng et al. (2011a,b) have shown that the interannual variation of the HC is closely linked with El Niño in both the boreal winter and summer, while interdecadal variations in the HC are

connected to a warming of the Indo-Pacific warm pool (IPWP). A recent study by Stachnik and Schumacher (2011) reported that significant strengthening of HC is seen in El Niño events relative to ENSO neutral and La Niña events during boreal winter. These studies highlight the important contribution of ENSO to variations in the HC.

However, it has been increasingly recognized that there are different flavors of ENSO that occur in the tropical Pacific (Wang and Weisberg 2000; Trenberth and Stepaniak 2001). Subsequently, it is suggested that there are two different types of ENSO (Larkin and Harrison 2005; Ashok et al. 2007; Yu and Kao 2007; Kao and Yu 2009; Kug et al. 2009). Recent studies have shown that canonical El Niño has become less frequent and a different kind of El Niño has become more common during the late twentieth century (Ashok et al. 2007; Kao and Yu 2009; Kug et al. 2009; Lee and McPhaden 2010) and in the future warming world based on some projections of phases 3 and 5 of the Coupled Model Intercomparison Project (CMIP3 and CMIP5, respectively; Yeh et al. 2009; Kim and Yu 2012). The study of Yu and Kao (2007) raised the possibility that interannual SST variability in the central and eastern Pacific Ocean may involve different physical processes. The canonical El Niño pattern corresponds to the leading mode of an empirical orthogonal function (EOF) analysis performed using tropical Pacific Ocean sea surface temperature anomalies (SSTA) (e.g., Rasmusson and Carpenter 1982; Trenberth 1997; Zhang et al. 2009). The second mode of tropical Pacific Ocean variability is dependent on the study period. An EOF performed on tropical Pacific SSTA for time series longer than 50 yr (i.e., 1880–2007 and 1948–2007) yielded a cooling mode in the equatorial Pacific cold tongue (Zhang et al. 2010). However, for the post-1970s period (i.e., 1979–2004) the second mode is represented by a warm SSTA located in the central Pacific, accounting for approximately 12% of the total variance (Ashok et al. 2007; within 30°S–30°N). This mode corresponds to the third SST mode for long-term variability (i.e., 1880–2007 and 1948–2007) in Zhang et al. (2010) over the tropical Pacific in the same domain. This mode, termed the date line El Niño (Larkin and Harrison 2005), El Niño Modoki (Ashok et al. 2007), the warm pool El Niño (Kug et al. 2009; Ren and Jin 2011), or the central Pacific El Niño (Kao and Yu 2009; Yu and Kim 2010), is characterized by warm SSTs near the international date line (Yu and Kao 2007; Kao and Yu 2009). Given the lack of consensus regarding the terminology used to refer to this new type of El Niño, we employ the term ''El Niño Modoki'' in this study.

Ashok et al. (2007) reported that El Niño Modoki is associated with a tripolar pattern of sea level pressure (SLP) anomalies during its evolution. They also documented the presence of two anomalous Walker circulation cells in the troposphere, instead of the single cell associated with the typical El Niño mode. The joint ascending branch of this double Walker circulation is located over the central equatorial Pacific, and the western/eastern descending branch is located over Indonesia and northern Australia/eastern Pacific. A consistent result is also reported in other studies (e.g., Weng et al. 2007, 2009; Taschetto and England 2009; Feng and Li 2011; Zhang et al. 2011). Subsequently, the influences on the regional climate particularly those of canonical ENSO and ENSO Modoki (EM) have been intensely studied, and it is reported that this configuration appears to influence regional climate (e.g., Weng et al. 2007, 2009; Taschetto and England 2009; Feng and Li 2011; Zhang et al. 2011, 2012; Afzaal et al. 2013) and the tropical tropopause layer and stratosphere (Xie et al. 2012) in a different way to that of a typical El Niño. For example, Weng et al. (2007, 2009) analyzed three El Niño Modoki events with the aim of assessing their influence on climate over China, Japan, and the United States during the boreal summer [June–August (JJA)] and winter (DJF). Taschetto and England (2009) examined the influence of El Niño Modoki on rainfall variability during the Australian autumn [March–May (MAM)], revealing that MAM is the time of maximum rainfall anomalies induced by El Niño Modoki over Australia. Cai and Cowan (2009) investigated the influence of La Niña Modoki on Australian autumn (MAM) rainfall, showing that the difference between the influence of ENSO and EM on Australian rainfall is most conspicuous during this period. Feng and Li (2011) indicated that the impacts of EM and ENSO on boreal spring (MAM) rainfall over south China are opposite and that significant influences only exist during warm events; this situation is also observed in the boreal autumn (Zhang et al. 2011) and boreal summer but over the Yangtze River valley (Afzaal et al. 2013). Yu and Kim (2011) explored the interactions between the EM/ENSO and the extratropical atmospheric phenomenon North Pacific Oscillation (NPO) and explained why strong El Niño events that usually occur in the eastern Pacific tend to be followed by strong La Niña events in the central Pacific. These results indicate that the two types of ENSO differ not only in the location of maximum SSTA but also in tropical–midlatitude teleconnections (Li et al. 2013).

The tropical Pacific SST mode EM was recognized only recently (Ashok et al. 2007); it remains unclear whether the tropical SSTA associated with EM has an influence on HC. As suggested in Yu and Kim (2010) that the central Pacific El Niño is more related to the

interaction between HC and the tropical Pacific, it is of interest to illustrate the potential influence of EM on HC. If such an influence exists, it would be important to consider the differences in its influence on HC during EM and during typical ENSO events. As reported in the context and shown in Fig. 1, we find that SSTA, particularly the zonal-mean SSTA structure, associated with the two types of ENSO shows the largest difference during the boreal spring, which has an important impact on the HC (Lindzen and Nigam 1987; Hou and Lindzen 1992; Feng et al. 2013); thus, we will focus on boreal spring in this study. Accordingly, one of the key goals of the present study is to investigate and compare the possible influences of ENSO and EM on the boreal spring HC. The remainder of this manuscript is organized as follows. Section 2 describes the datasets, methods, and model used in this study, and section 3 outlines the possible influences of EM and a typical ENSO on the HC during MAM. Section 4 presents the results of numerical modeling of EM- and ENSO-associated warming on the HC. Finally, conclusions and a discussion are provided in section 5.

## 2. Datasets, methods, and model

### a. Observational datasets

The atmospheric fields are from the National Centers for Environmental Prediction–National Center for Atmospheric Research (NCEP–NCAR) reanalysis (Kalnay et al. 1996), with 17 vertical levels and on a 2.5° × 2.5° latitude–longitude grid (http://www.esrl.noaa.gov/psd/data/gridded/data.ncep.reanalysis.html). Given the inconsistencies among different reanalyses and the potential biases in NCEP–NCAR (Zhao and Li 2006; Stachnik and Schumacher 2011; Feng et al. 2013), the 40-yr European Centre for Medium-Range Weather Forecasts (ECMWF) Re-Analysis (ERA-40) from 1979 to mid-2002 (Uppala et al. 2005) is further employed to examine the circulation anomalies associated with the two types of ENSO. Three SST datasets are extracted from the Improved Extended Reconstruction of SST (IERSST; Smith and Reynolds 2004) on a 2° × 2° latitude–longitude grid; the Hadley Centre Sea Ice and SST (HadISST) dataset, version 1, on a 1° × 1° latitude–longitude grid (Rayner et al. 2003); and the Kaplan SST dataset on a 5° × 5° latitude–longitude grid (Kaplan et al. 1998) to further verify the result. Considering that EM has occurred mainly since the late 1970s (Ashok et al. 2007), we focused on the period 1979–2010, also for the climatology and the reference period.

### b. Methodology

In this study, four widely used methods are employed to depict the characteristics of HC accompanied with ENSO and EM. First, the zonal-mean meridional wind and vertical velocity is employed to depict the features of meridional circulation. Second, the mass streamfunction (MSF) of the mean meridional circulation is adopted. The MSF is obtained by vertically integrating meridional winds in the conventional way (Li 2001) and is defined by

$$\psi = \int \frac{2\pi a \cos\phi}{g} [\overline{v}]\, dp, \tag{1}$$

where $[\overline{v}]$ is the zonal-mean meridional wind, $a$ is the mean radius of the earth, $\phi$ is the latitude, $g$ is the gravitational acceleration, and $p$ is the pressure. The overbar and square brackets represent temporal and zonal averaging, respectively.

In addition, considering that velocity potential at 200 hPa contains information concerning the overall intensity of the tropical circulations, HC is defined as the axisymmetric part of the circulation as in Tanaka et al. (2004). Negative values indicate rising, and positive is for descending. Besides, the vertical shear of zonal-mean divergent meridional wind at 200 and 850 hPa is used as a factor to reflect the overturning of meridional circulation (Oort and Yienger 1996) and to examine HC anomalies associated with ENSO and EM. A positive component is associated with an overturning circulation that has northward motion at 200 hPa and southward motion at 850 hPa.

Following Ashok et al. (2007), the ENSO Modoki index (EMI) is defined as

$$\mathrm{EMI} = [\mathrm{SSTA}]_C - 0.5 \times ([\mathrm{SSTA}]_E + [\mathrm{SSTA}]_W),$$

where square brackets with a subscript represent the areal-mean SSTA over the central Pacific region $C$ (10°S–10°N, 165°E–140°W), eastern Pacific region $E$ (15°S–5°N, 110°–70°W), and western Pacific region $W$ (10°S–20°N, 125°–145°E). The canonical ENSO is quantified by the Niño-3 index, which is defined as the areal-mean SSTA over the region (5°S–5°N, 150°–90°W) (Trenberth and Stepaniak 2001). These indices are based on HadISST and are departures from their respective means for the period 1979–2010.

The relation between ENSO/EM and HC is investigated by regression and composite analyses. Here, the composite analyses for an index are the differences between the strong (greater than plus one standard deviation of the index) and weak values (less than minus one standard deviation of the index). Note that the

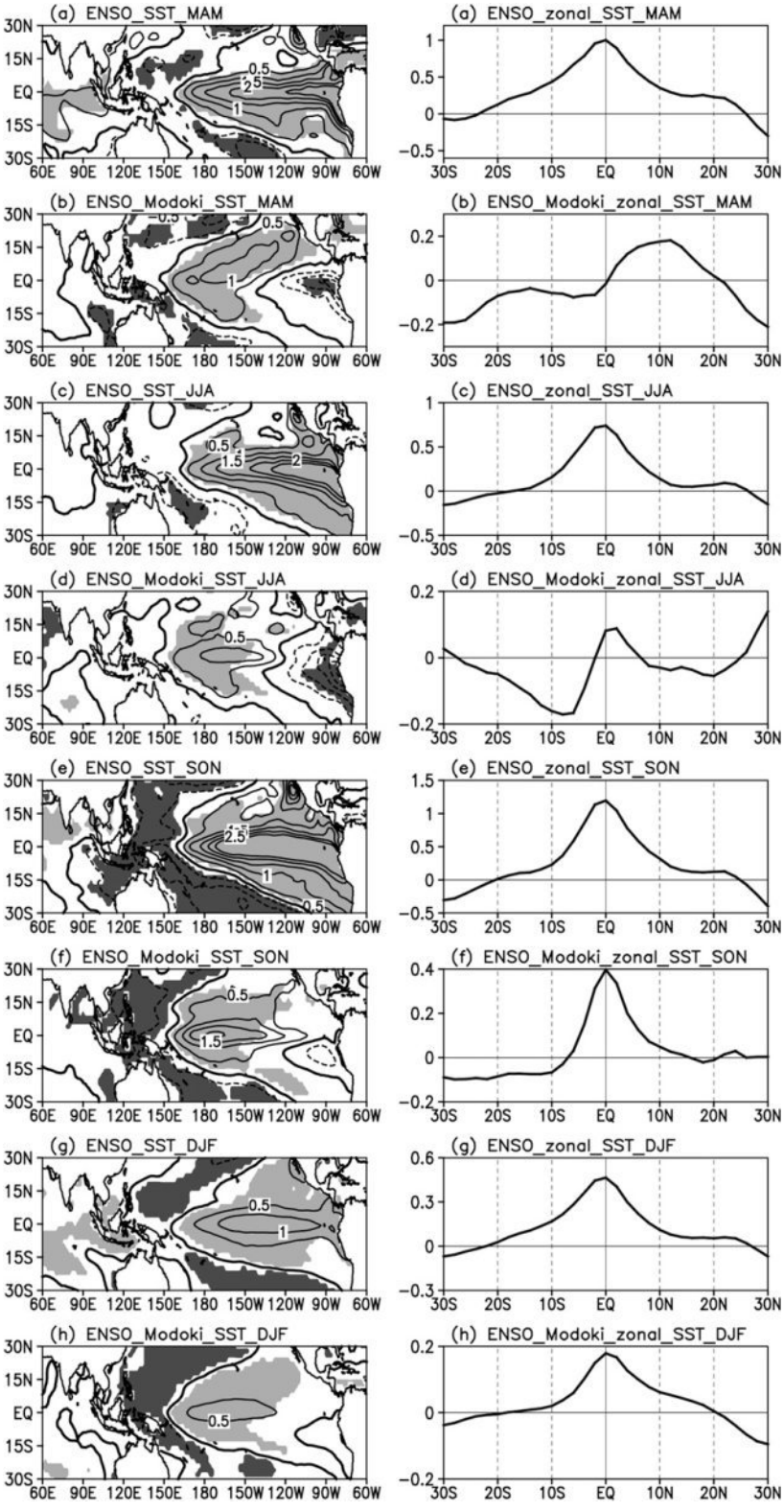


FIG. 1. Composite anomalies between El Niño/El Niño Modoki and La Niña/La Niña Modoki events during four seasons (DJF, MAM, JJA, and SON) in terms of [left, (a)–(h)] the distribution of SST and [right, (a)–(h)] zonal-mean SST (°C). Shading indicates statistical significance at the 0.1 level.

TABLE 1. The warm and cold years for El Niño (El Niño Modoki) and La Niña (La Niña Modoki).

| | ENSO | | | | ENSO Modoki | | | |
|---|---|---|---|---|---|---|---|---|
| | MAM | JJA | SON | DJF | MAM | JJA | SON | DJF |
| Warm | 1983 | 1982 | 1982 | 1982 | 1982 | 1991 | 1990 | 1979 |
| | 1987 | 1983 | 1987 | 1991 | 1991 | 1994 | 1991 | 1990 |
| | 1992 | 1987 | 1997 | 1997 | 1994 | 2002 | 1994 | 1994 |
| | 1993 | 1997 | | 2009 | 1995 | 2004 | 2004 | 2004 |
| | 1998 | 2009 | | | 2003 | | 2009 | 2009 |
| Cold | 1985 | 1985 | 1988 | 1984 | 1983 | 1983 | 1983 | 1988 |
| | 1989 | 1988 | 1999 | 1988 | 1989 | 1997 | 1988 | 1997 |
| | | 2010 | 2007 | 1999 | 1998 | 1998 | 1997 | 1998 |
| | | | 2010 | 2007 | 1999 | 1999 | 1998 | 1999 |
| | | | | | 2000 | 2008 | 2008 | 2000 |
| | | | | | 2001 | | 2010 | 2007 |
| | | | | | 2008 | | | 2008 |

seasonal-averaged index values are used to show the composite differences associated with the two types of ENSO in each season. The warm and cold events for the two types of ENSO in each season for the composite are listed in Table 1. For each season, the cases for composite are at least larger than 2, indicating that the result would not be biased by a single event in both types of ENSO. The statistical significance of values of the correlation and composite are accessed by means of a two-sided Student's *t* test. Besides, the spatial correlation is employed to show the different influence of ENSO and EM on the anomalous fields between the regression patterns with respect to ENSO and EM, respectively.

### c. Model

The atmospheric general circulation model used in this study is the NCAR Community Atmospheric Model, version 3.0 (CAM3; Collins et al. 2006), which is able to reproduce the climate features as observed (e.g., Feng et al. 2012; Li et al. 2012). The CAM is the latest in a series of global atmospheric models developed at NCAR for weather and climate research communities, and serves as the atmospheric component of the Community Climate System Model (CCSM). The horizontal resolution is T42 (approximately 2.8° latitude × 2.8° longitude), with 26 hybrid vertical levels (for a detailed description of this model version, see http://www.ccsm.ucar.edu/models/atm-cam/docs/description/).

## 3. Influence of ENSO and EM on the boreal spring HC

Figure 1 shows the anomalous SST associated with ENSO and EM during four seasons, as well as their zonal-mean distributions. Positive SSTA in the eastern Pacific and negative anomalies in the western Pacific are observed in all seasons [i.e., DJF, MAM, JJA, and September–November (SON)] associated with El Niño events. El Niño Modoki is characterized by warm SSTA in the central Pacific flanked by cool SSTA in the western and eastern Pacific. The zonal-mean SSTA during El Niño events shows a quasi-symmetrical structure within the tropics in all seasons, with the maximum around the equator. Similar features are observed in El Niño Modoki cases during JJA, SON, and DJF but not in MAM. The maximum SSTA in MAM is around 10°N, with positive anomalies to the north of the equator and negative anomalies to the south of the equator within the tropics, similar to the reported meridional mode of SSTA (Chiang and Vimont 2004). Note that the anomalies associated with the warm and cold events for the two types of ENSO were separately examined (figures not shown), and we found that the SSTA in the cold events are almost opposite to the warm events. Particularly, the equatorial asymmetric structure during the boreal spring is observed in both the warm and cold events of the EM, indicating almost symmetric influences of warm and cold events. The above result indicates that the meridional SST gradient during MAM associated with EM is different from that associated with ENSO, suggesting that ENSO and EM may have different impacts on the boreal spring HC. Note that similar zonal-mean SSTA patterns are observed even if the period 1948–2010 is examined (figure not shown), indicating the associated SSTA pattern is stable and not be biased by some strong events. In addition, another two SST datasets are employed to further establish the above result. The biggest differences during the boreal spring in the meridional distribution of SSTA associated with the two types of ENSO are consistently observed (Fig. 2), indicating the result in the boreal spring is reliable. In contrast, although the meridional structure of SSTA associated with the two types of ENSO shows certain asymmetric differences during the boreal summer, it is inconsistently

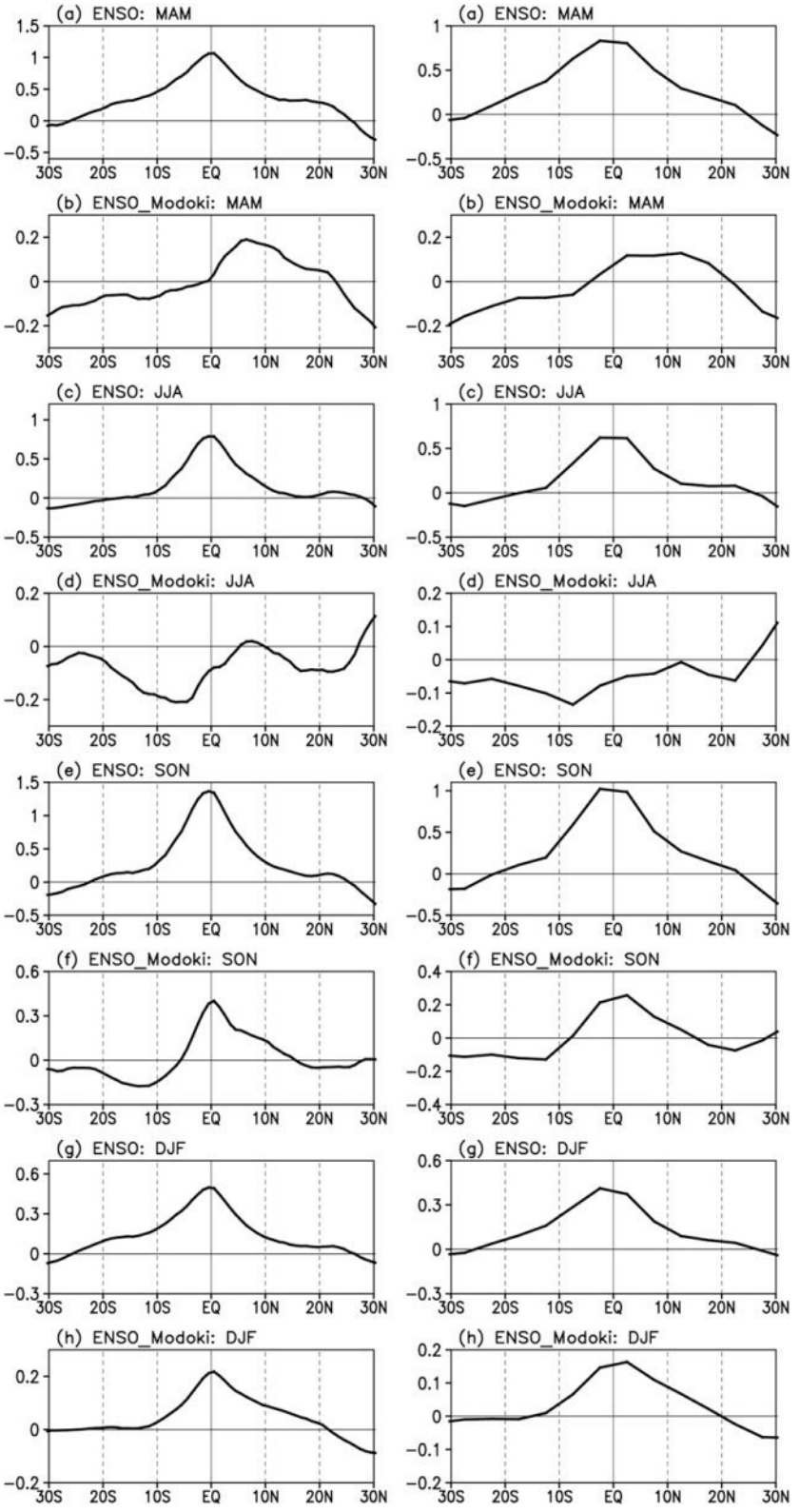


FIG. 2. Composite anomalies between El Niño/El Niño Modoki and La Niña/La Niña Modoki events during four seasons in terms of the zonal-mean SST (°C) based on [left, (a)–(h)] HadISST and [right, (a)–(h)] Kaplan SST.

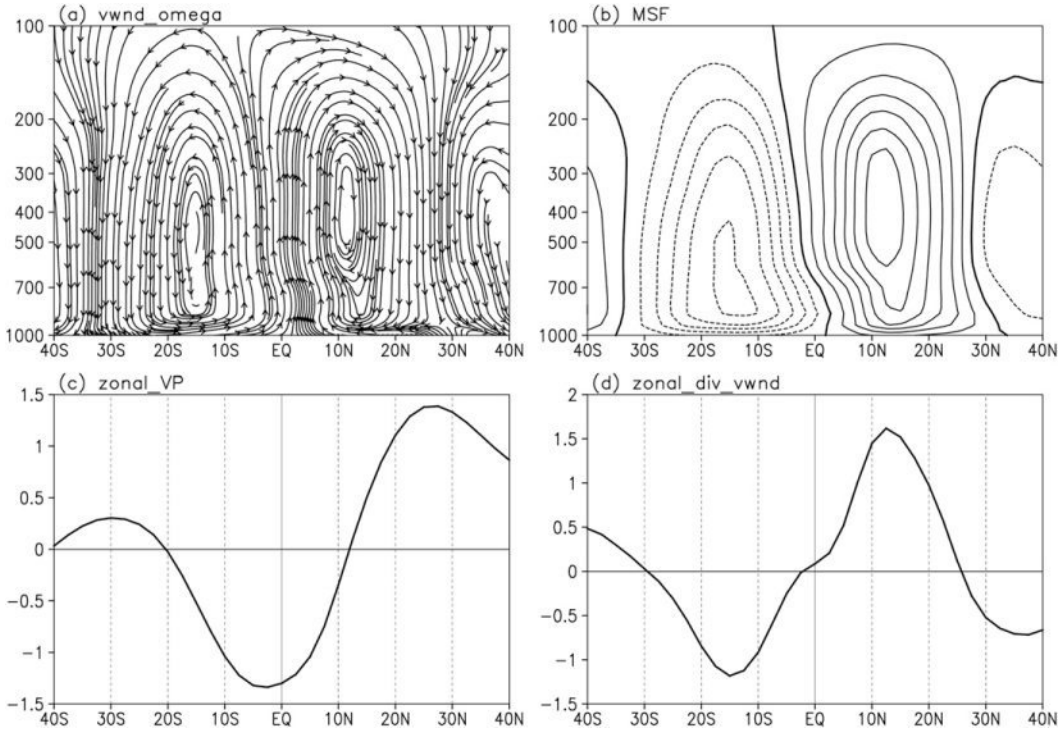


FIG. 3. Boreal spring climatology for the period 1979–2010, showing (a) zonal-mean meridional circulation, (b) MSF [contour interval (CI) is $1.5 \times 10^{10}$ kg s$^{-1}$; zero contour is thick], (c) zonal-mean velocity potential at 200 hPa ($10^6$ m$^2$ s$^{-1}$), and (d) zonal-mean vertical shear of divergent meridional wind between 200 and 850 hPa (m s$^{-1}$).

seen in the three SST datasets. This indicates that the result in the boreal summer is not identifiable as the result in the boreal spring. As for the boreal autumn and winter, despite the consistent SSTA patterns that are observed within the three SST datasets, the SSTAs associated with both ENSO and EM are found to be equatorially symmetric. This suggests that the meridional gradient of SSTA associated with the two types of ENSO during boreal autumn and winter are similar, which in turn raises the possibility that their impact on HC may be more difficult to distinguish. Furthermore, previous studies have already shown that the distribution of the meridional SST gradient plays an important role in influencing the spatial structure of HC (Lindzen and Nigam 1987; Hou and Lindzen 1992; Feng et al. 2013). Hereafter, we will focus on the boreal spring and investigate the possible influences of ENSO and EM on the simultaneous HC.

The normal structure of HC during the boreal spring is given in Fig. 3 as a reference to show the background setting and to reveal the differences between ENSO and EM events. Considering the four methods used to characterize the structure of HC, we see that the southern and northern components of HC show equivalent magnitudes and extents, with an upward branch around the equator and subsidence around 30° in each hemisphere.

To provide insight into HC variations associated with ENSO and EM, we investigate changes in HC using composite differences of warm and cold events in both ENSO and EM (Fig. 4). The warm and cold events of ENSO/EM have opposite signs but identical climatic impacts. Thus, in the following discussion we refer to the warm-minus-cold composite differences as anomalous conditions to the warm events (i.e., El Niño and El Niño Modoki); similarly anomalous conditions associated with cold events (i.e., La Niña and La Niña Modoki) can be approximated as the reverse of the warm-minus-cold situation.

There exist distinct differences between the warm-minus-cold events in both ENSO and EM. In the case of El Niño, a pair of anomalous equatorial symmetric meridional circulations is observed, with the conjunct rising branch around the equator. In the Northern Hemisphere there is an obvious anomalous clockwise meridional circulation with a descending branch located at about 15°N (Fig. 4a). Of note, the northern anomalous meridional circulation is much stronger than its counterpart in the Southern Hemisphere, possibly because

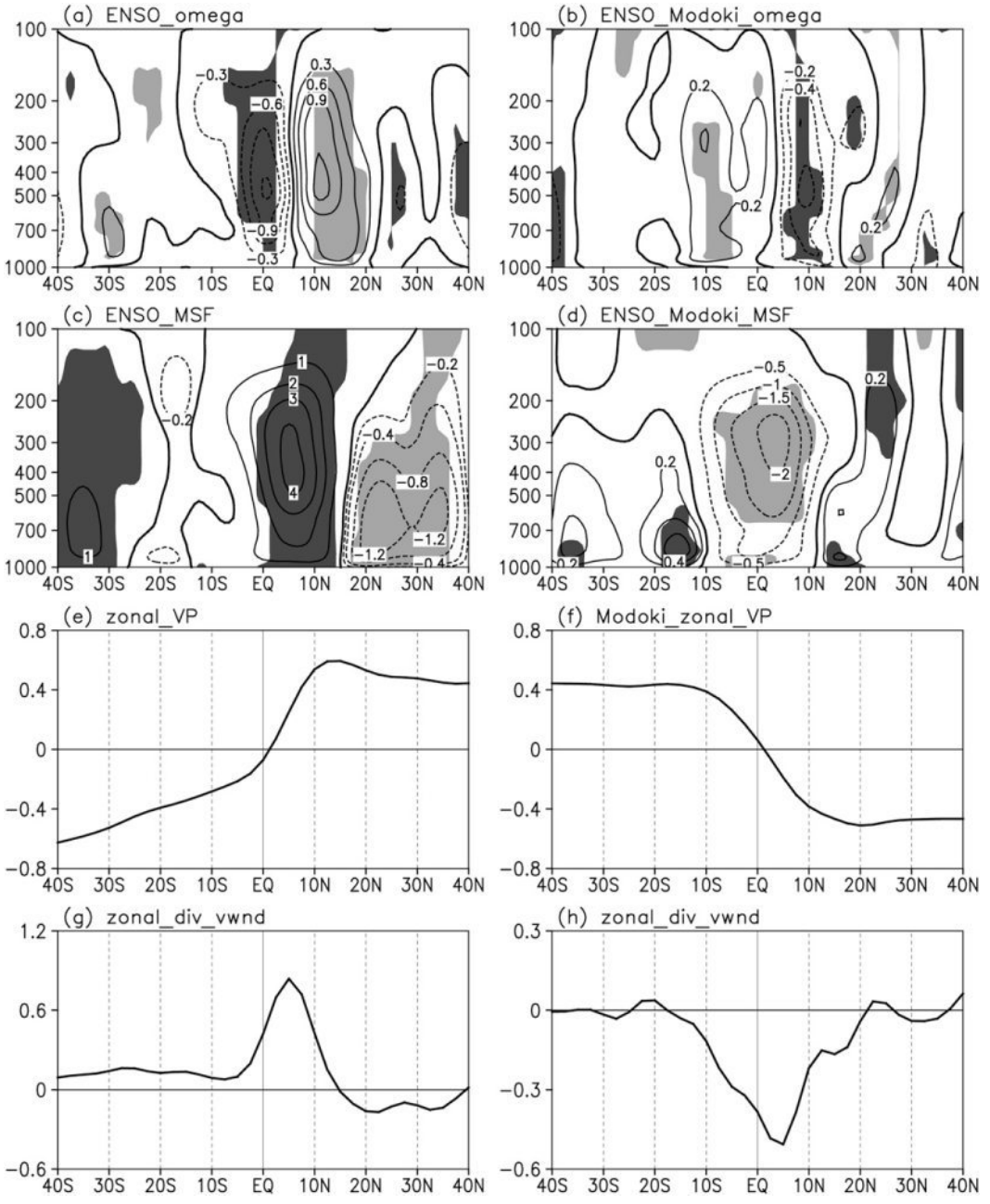


FIG. 4. As in Fig. 1, but for the composite differences of (a),(b) zonal-mean vertical velocity ($10^{-2}$ m s$^{-1}$); (c),(d) mass stream function ($10^{10}$ kg s$^{-1}$); (e),(f) zonal-mean velocity potential at 200 hPa ($10^{6}$ m$^{2}$ s$^{-1}$); and (g),(h) zonal mean of the vertical shear of divergent meridional wind between 200 and 850 hPa (m s$^{-1}$). Shading indicates statistically significant at the 0.2 level.

1) the zonal-mean anomalous SST within 10°S–0° is more intense than that within 0°–10°N (0.73°C versus 0.66°C) and 2) the slope of the SSTA in the Northern Hemisphere (0°–10°N) is steeper than that in the Southern Hemisphere (10°S–0°). The former helps to induce a stronger rising branch in the Southern Hemisphere, as shown in Fig. 4a; the latter results in a stronger meridional circulation in the Northern Hemisphere, as indicated by Hou and Lindzen (1992). Similar results are also observed in the other three measures that are characteristic of HC. For example, anomalous rising is seen around and to the south of the equator (Figs. 4c,e), while

descent is seen around 15°N. Accompanying these changes are anomalous southerlies in the upper levels of the troposphere and northerlies in the lower troposphere within 0°–15°N (Figs. 4a,g). This result suggests that HC in the Northern Hemisphere is intensified during El Niño events, as indicated by Quan et al. (2004) but for boreal spring. The rising is particularly enhanced around the equator. This interpretation is further verified by the robust relationships between the Niño-3 index and the zonal-mean vertical velocity in the lower troposphere (averaged from 925 to 700 hPa) within 10°S–0° and 5°–15°N, which yield correlation coefficients of −0.52 and 0.69, respectively.

In contrast, an equatorial asymmetric vertical meridional circulation is observed during El Niño Modoki events, with anomalous ascent at 10°N and descent at about 10°S and 20°N (Fig. 4b). This is also seen in the other three measures of the meridional circulation (MSF: the axisymmetric part of the velocity potential at 200 hPa and the vertical shear of zonal-mean divergent wind between 200 and 850 hPa). Anomalous northerlies are found between 10°S and 10°N in the upper levels of the troposphere (Fig. 4h); an anticlockwise circulation is observed in the MSF (Fig. 4d). This result indicates that the rising branch of HC shifts northward in El Niño Modoki cases; rising around 10°N is enhanced and rising at 10°S is suppressed. This is further supported by the strong relationships between EMI and the zonal-mean vertical velocity within 0°–10°N and 10°S–0° in the lower troposphere (averaged from 925 to 700 hPa), which yield correlation coefficients of −0.57 and 0.35 (both significant at the 0.05 level). The situation associated with El Niño Modoki is clearly opposite to that during El Niño events. Note that the strength of the anomalous meridional circulation associated with EM is smaller than that with ENSO, reflecting the fact that the warm SST area in the tropical Pacific, which forces the atmospheric anomalies, is less intense during El Niño Modoki events (Bulic and Brankovic 2007). Note that the composite differences based on the ERA-40 is similar to the above result based on the NCEP–NCAR reanalysis, except that the anomalous meridional circulation associated with ENSO is a bit more equatorial symmetric than observed from NCEP–NCAR, implying that the result here is reliable (figure not shown).

The above results indicate contrasting anomalous meridional circulation associated with ENSO and EM within the tropics. This point is further supported by the spatial correlation coefficients between the anomalous regression patterns with respect to the Niño-3 index and EMI, as listed in Table 2. Negative spatial correlation coefficients are obtained between the anomalous circulation patterns associated with ENSO and EM in MSF, zonal-mean meridional wind, zonal-mean vertical velocity, and vertical shear of divergent wind between 200 and 850 hPa. Note that the opposite impacts of ENSO and EM on the meridional circulation are not only seen within the tropics but also in the extratropical regions. This result further indicates that the anomalous meridional circulation that accompanies ENSO and EM is opposite in each case during the boreal spring. It should be emphasized that the horizontal extensions of the anomalous meridional circulation associated with ENSO and EM reach one-half of that seen in a normal HC during the boreal spring, as shown in Fig. 3 (~30° latitude versus ~60° latitude). This result suggests that both EM and canonical ENSO have important influences on the HC.

TABLE 2. Spatial correlation coefficients between anomalous regression patterns with respect to the Niño-3 index and EMI during MAM for the period 1979–2010. Note the following: 1) MSF represents the mass streamfunction from 1000 to 100 hPa; 2) $v$ represents the vertical regression pattern of the zonal-mean meridional wind from 1000 to 100 hPa with respect to the Niño-3 index and EMI; 3) $\omega$ represents the vertical regression pattern of the zonal-mean vertical velocity from 1000 to 100 hPa with respect to the Niño-3 index and EMI; 4) $vd$ represents the regression pattern of the vertical shear of the divergent meridional wind between 200 and 850 hPa with respect to the Niño-3 index and EMI; and 5) $\chi 200$ represents the regression pattern of the velocity potential at 200 hPa with respect to the Niño-3 index and EMI.

| | MSF | $v$ | $\omega$ | $vd$ | $\chi 200$ |
|---|---|---|---|---|---|
| 60°S–60°N | −0.70 | −0.63 | −0.49 | −0.72 | −0.24 |
| 50°S–50°N | −0.72 | −0.65 | −0.50 | −0.72 | −0.23 |
| 40°S–40°N | −0.74 | −0.67 | −0.61 | −0.75 | −0.23 |
| 30°S–30°N | −0.80 | −0.74 | −0.67 | −0.74 | −0.26 |

The above analyses show that the contributions of warm events in ENSO and EM to the boreal spring HC are opposite. That is, in warm ENSO events, the rising around the equator is enhanced, whereas that at about 10°N is suppressed; in warm EM events, in contrast, the rising at about 10°N is intensified and the rising in the Southern Hemisphere (at about 10°S) is weakened. This pattern arises because the underlying thermal structure differs between ENSO and EM, as shown in Figs. 1a,b. This result is further supported by the work of Lindzen and Nigam (1987), who illustrated that SST gradient forcing is an important mechanism for lower-level tropical flow and convergence, and they described a zonally symmetric model to determine the lower-tropospheric HC that is forced by SST alone. Their model equations are as follows:

$$f\overline{V} = \varepsilon\overline{U}, \tag{2}$$

$$f\overline{U} = -\left\{(2 - n\overline{T_s} + n\alpha H_0)\frac{\partial \overline{h}}{\partial \varphi} - \frac{nH_0}{2} - \frac{\partial \overline{T_s}}{\partial \varphi}\right\} - \varepsilon \overline{V}, \quad \text{and} \tag{3}$$

$$\overline{h} = \frac{H_0 \tau_c}{a \cos\theta}\left\{\frac{\partial(\overline{V}\cos\theta)}{\partial \theta}\right\}, \tag{4}$$

where $u$ and $v$ are the zonal and meridional velocity, respectively; $f$ is the variable Coriolis parameter; $h$ is the modulation of the boundary layer height; $\varepsilon$ and $n$ are the coefficients of turbulent friction and air expansion, respectively; $H_0$ is the height of the boundary layer; $a$ is the radius of the earth; $T_s$ is the SST field; $U$ is the zonal wind; $V$ is the meridional wind; $\theta$ is the longitude; $\alpha$ is the vertical lapse rate of air temperature; and the overbar denotes a zonal mean. As pointed by Lindzen and Nigam (1987), this model is unable to well simulate the zonal flow, because of the neglect of the effects of any stresses on the low-level zonally symmetric circulation from HC above the trade inversion, but the simulation of the zonal-mean meridional wind is fine. Subsequently, other studies reported that HC is sensitive to the profiles and position of the external heating (Lindzen and Hou 1988; Chao and Wang 1991). Accordingly, we can diagnose the relationship between SST and meridional wind by (2) $\times f +$ (3) $\times \varepsilon$, and taking account that $h$ equals zero in the equilibrium condition as follows:

$$\overline{V} \propto \frac{\partial \overline{T_s}}{\partial \varphi}. \tag{5}$$

This relation between zonal-mean SST and meridional wind indicates that meridional wind is subjected to the underlying meridional thermal gradient. That is, the positive (negative) meridional SST gradients are associated with southerlies (northerlies). Therefore, the position where the SST meridional gradient equals zero and varies from positive to negative, paralleling the location of convergence, is identical to the position of the upward branch of HC. To further validate the relationship between the meridional SST gradient and meridional wind, we first checked the situation in the climatology. It is found that the position where the gradient crosses zero is around the equator and overlaps the location of the ascending branch of the MAM HC (figure not shown). This result suggests that the above simplification is reasonable.

To strengthen this point, Fig. 5 shows the meridional gradient of SSTA associated with El Niño (Modoki) and La Niña (Modoki) events (the data are smoothed using a 5-point moving average employing the central difference method). The position where the meridional gradient of SSTA equals to zero, located at the equator in the El Niño case (Figs. 5a,c,e), is consistently seen in the three SST datasets and is accordant with the result in Fig. 4a. However, it is located at about 10°N in El Niño Modoki events (Figs. 5b,d,f), indicating that the opposite influences of ENSO and EM on the boreal spring HC are caused by their accompanying SST structure. In addition, there is another location that the zonal-mean SSTA gradient varies from positive to negative around 13°S in the EM case (Fig. 5b) in the ERSST; however, this cannot be observed in the HadISST and Kaplan SST datasets. The inconsistency implies that the negative values here are not reliable or persistent and that their amplitude is much smaller than those around 10°N; consequently, they are not considered in this study.

To further test the above result regarding the anomalous SST structures associated with EM and ENSO and show a quantitative representation of the symmetric and asymmetric variations of the tropical SST, two simple meridional gradient indices of zonal-mean tropical SST are employed to examine the possible linkage between SST variations and the two types of ENSO. The SST indices are named the meridional symmetric SST index (MSSI) and the meridional asymmetric SST index (MASI) to represent the equatorially symmetric and asymmetric tropical SST variations in the meridional direction, respectively. The MSSI and MASI are defined as follows:

$$\mathrm{MSSI} = \mathrm{SSTA}_{(5°\mathrm{S}-5°\mathrm{N})} - 0.5 \times \left\{\mathrm{SSTA}_{(15°\mathrm{S}-5°\mathrm{S})} + \mathrm{SSTA}_{(5°-15°\mathrm{N})}\right\} \quad \text{and} \tag{6}$$

$$\mathrm{MASI} = \mathrm{SSTA}_{(5°-15°\mathrm{N})} - \mathrm{SSTA}_{(15°-5°\mathrm{S})}. \tag{7}$$

These indices measure the symmetric and asymmetric variations of the tropical SST, respectively. The correlation distribution between the two SST indices and the SST field (Fig. 6) shows that the symmetric SST index (i.e., MSSI) mainly reflects the characteristics associated with El Niño. In contrast, the asymmetric SST index (i.e., MASI) is linked to the SST pattern of El Niño Modoki. This result is further verified by the robust correlations between MSSI (MASI) and the Niño-3 index (EMI) [i.e., $R$(MSSI, Niño-3 index) = 0.94 and $R$(MASI, EMI) = 0.63]. This finding indicates that ENSO generally represents the equatorially symmetric part of tropical SST variations, and EM corresponds with the asymmetric part of SST during the boreal spring. It follows that equatorially symmetric and asymmetric meridional circulation anomalies are observed during El Niño and El Niño Modoki events, respectively.

The above result is verified by the correlations between the MSSI/MASI and the zonal-mean vertical circulation as shown in Fig. 7. We see the asymmetric SST

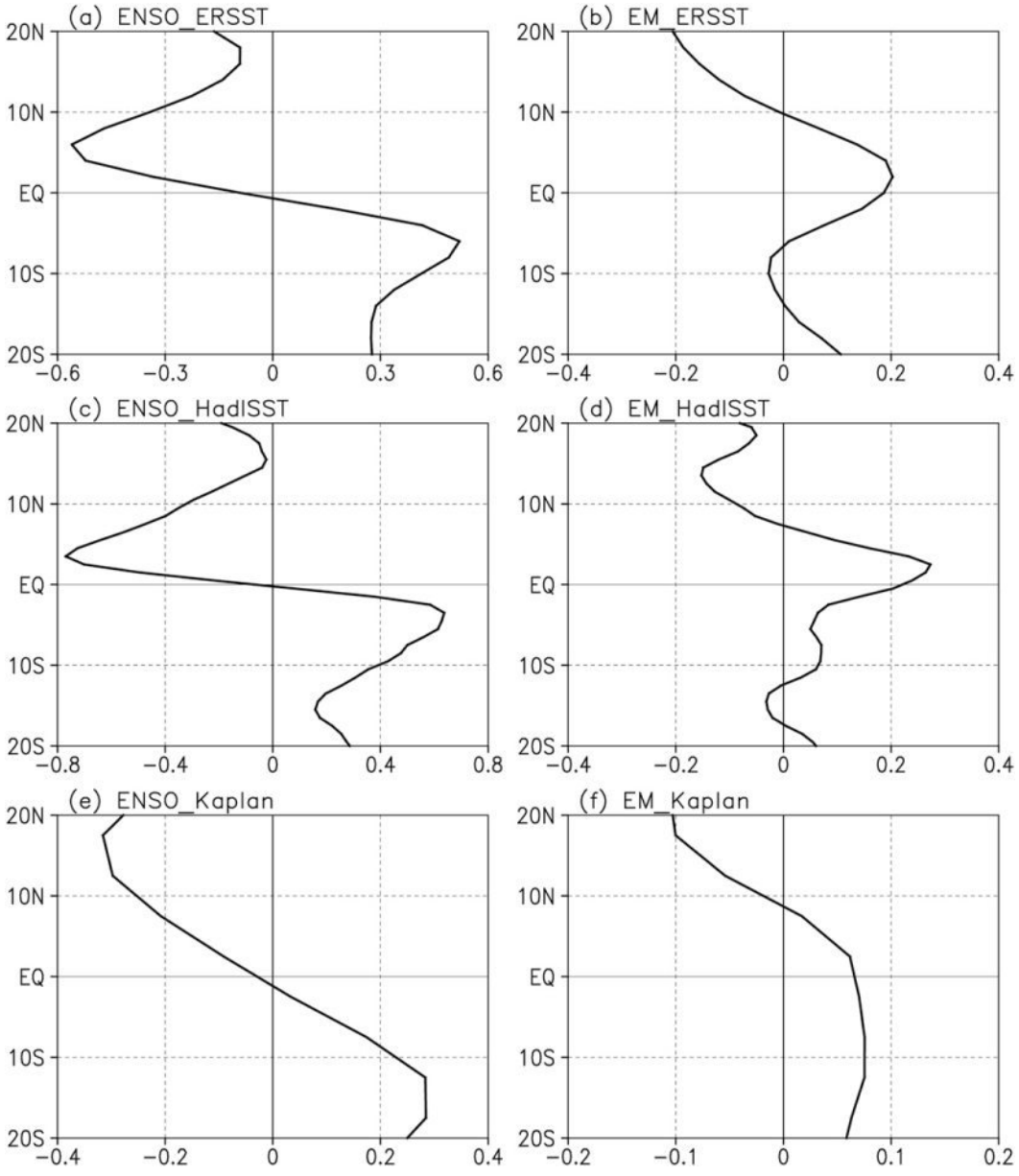


FIG. 5. (a) Meridional gradient of zonal-mean SST anomalies based on the difference between El Niño and La Niña events from ERSST. (b) As in (a), but for the distribution based on the difference between El Niño Modoki and La Niña Modoki events. (c),(d) As in (a),(b), but based on HadISST and Kaplan SST ($10^{-6}$ K m$^{-1}$). The data are smoothed using a 5-point moving average employing the central difference method.

variation is accompanied with an asymmetric meridional circulation, which is similar to those associated with El Niño Modoki events. Meanwhile, the symmetric SST variation is connected to equatorial symmetric meridional circulation, paralleling to those linked with El Niño events.

A further issue to be resolved is whether the impact of EM on HC is contaminated by other factors. Given the reported fact that variations of the equatorial asymmetric principal mode of HC variability in the boreal winter (Ma and Li 2007, 2008), summer (Feng et al. 2011b), and spring (Feng et al. 2013) are closely linked to variations of SST over the Indo-Pacific warm pool, the warming of the IPWP has contributed to interdecadal variations in HC. To examine this point (i.e., whether the impact of EM on the boreal spring HC is dependent on SST in the IPWP), Fig. 8 shows the partial correlation between EMI and MSF, zonal-mean vertical velocity,

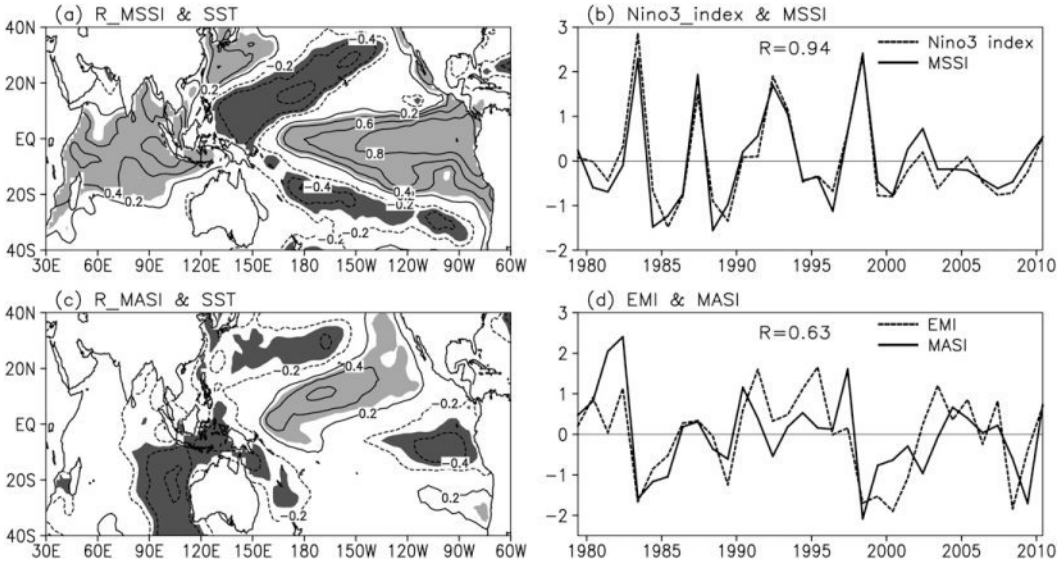


FIG. 6. (a) Correlation pattern between MAM SST and MSSI. (b) Normalized time series of Niño-3 index and MSSI. (c) As in (a), but for the correlation between MAM SST and MASI. (d) As in (b), but for EMI and MASI. Shading indicates statistical significance at the 0.1 level.

and meridional wind after removing the effect of SSTs over IPWP. Here the spatially averaged SST over 10°S–10°N, 60°–160°E is defined as the IPWP index (IPWPI) as in Feng et al. (2011a), to reflect the variation in SST over the IPWP. The anomalous meridional circulation associated with EM changed little after removing the effects of the IPWP, suggesting that the influence of EM on the boreal spring HC is largely independent of that of the IPWP.

## 4. Modeling results

To further examine the influences of ENSO and EM on variations of HC in the boreal spring, we performed numerical experiments with CAM3. A control run was integrated for 20 yr and was used to derive a reference state. A sensitivity experiment was integrated for 22 yr, with the latter 20 yr of integration being used to construct a 20-member ensemble mean to reduce the uncertainties arising from varying initial conditions. To isolate and reproduce the impact of SST variations on the circulation associated, the only difference between the control and sensitivity experiments is SST in the eastern and central Pacific during the boreal spring (see Fig. 9). Note that SST in the eastern and central Pacific are identical to the SSTA between the warm and cold events associated with the two types of ENSO events during MAM.

Figure 10 shows the ensemble-mean response of the zonal-mean meridional wind and vertical velocity in MAM. When forced by eastern Pacific warming (see Fig. 10a), the observed anomalous equatorial meridional

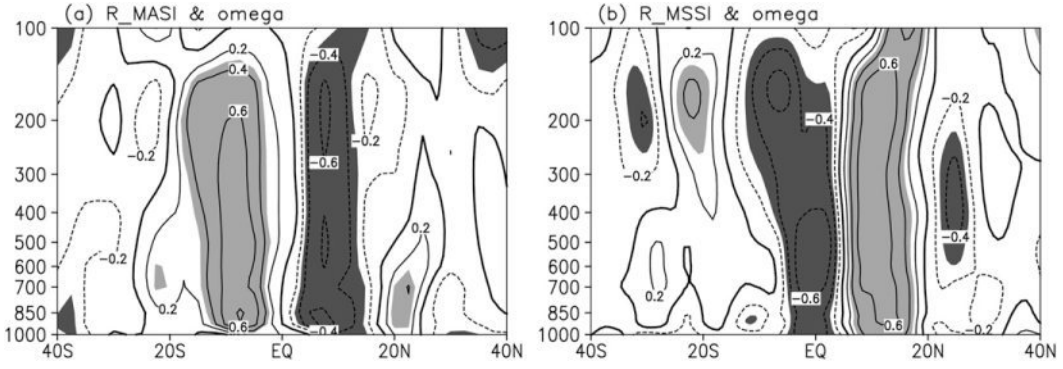


FIG. 7. (a) As in Fig. 6a, but for the latitude–height distribution of the correlation between MASI and zonal-mean vertical velocity. (b) As in (a), but for the correlation between MSSI and zonal-mean vertical velocity.

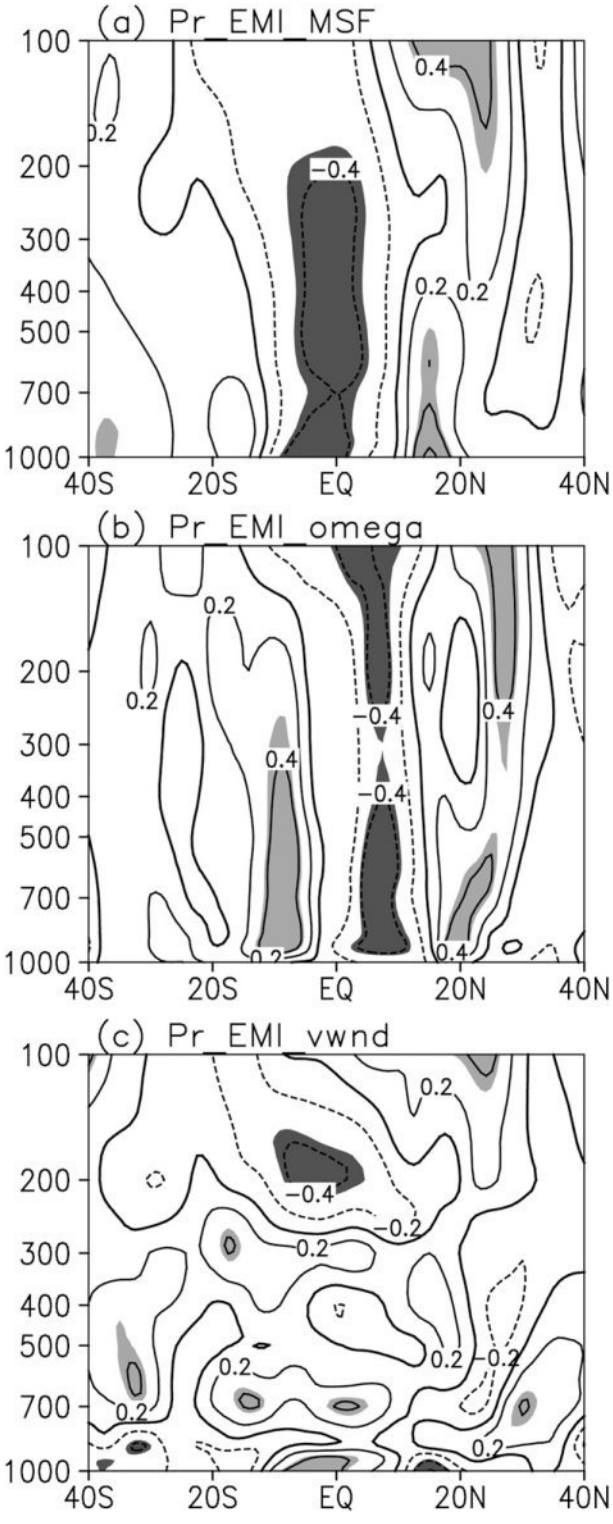


FIG. 8. As in Fig. 6a, but for the partial correlation between EMI and (a) MSF, (b) zonal-mean vertical velocity, and (c) zonal-mean meridional wind after removing the effects of SST over the IPWP.

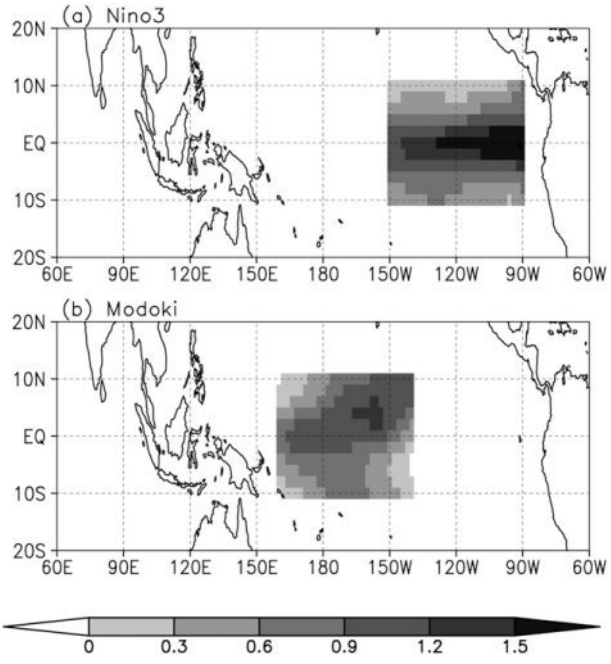


FIG. 9. Specified SSTA pattern used in the numerical simulations of (a) ENSO and (b) ENSO Modoki events (°C).

circulation is well captured by the simulation (Fig. 10a). The convergence and ascent over the equator is enhanced while descent around 15° is seen in both hemispheres (Figs. 10a,c). In terms of warming in the central Pacific, we see anomalous convergence and rising at about 10°N; the rising around 10°S and 20°N is suppressed (Figs. 10b,d). These characteristics, in response to anomalous warming in the eastern and central Pacific, are similar to those seen in the observations. The consistency between the observations and model results further verifies that the eastern and central Pacific warming associated with El Niño and El Niño Modoki events induces opposite impacts on boreal spring HC. Of note is that similar anomalous meridional circulation is observed where the tropical zonal SSTA patterns associated with the two types of ENSO are used as the forces to perform the experiments (figures not shown). Therefore, the contrasting SSTA patterns associated with the two types of ENSO lead to different responses in the meridional circulation.

## 5. Discussion and conclusions

Using recent 32-yr observational datasets, we have demonstrated that the boreal spring is the most conspicuous season in which the biggest differences in zonal-mean SSTA are consistently observed between ENSO and EM in the three SST datasets. Furthermore, boreal spring HC is influenced by both typical ENSO

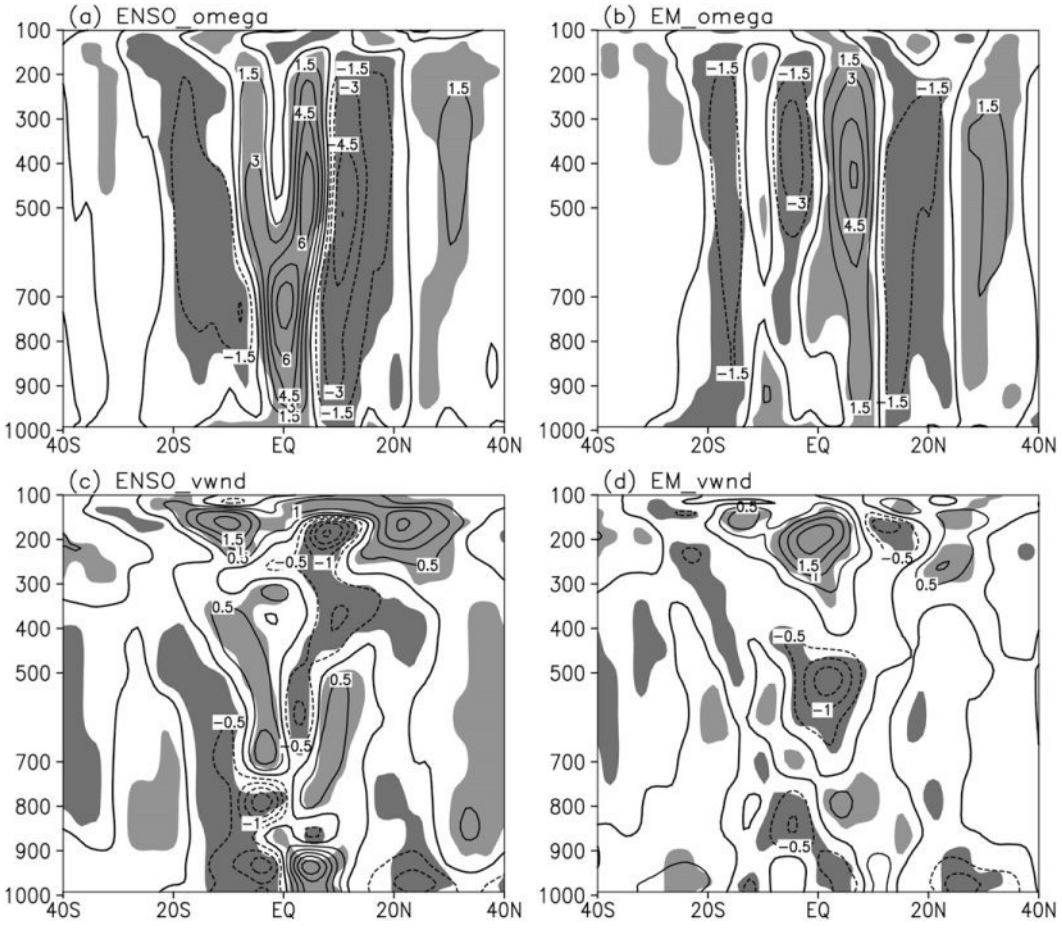


FIG. 10. Ensemble-mean response of the zonal-mean vertical velocity to warming in the (a) eastern (ENSO) and (b) central Pacific (EM) during MAM. (c),(d) As in (a),(b), but for the ensemble-mean response of the zonal-mean meridional wind. Shading indicates statistical significance at the 0.1 level.

events and by the newly recognized EM. Both phenomena play important roles in influencing HC but with contrasting impacts that reflect their different underlying thermal structures, particularly in the zonal-mean structure of their SSTA. In El Niño events, the anomalous SST shows an equatorially symmetric pattern with the maximum around the equator, whereas the maximum SSTA in El Niño Modoki events is located around 10°N. These anomalous SST patterns induce different anomalous meridional gradients in zonal-mean SSTA, which in turn have reversed impacts on HC. This result is further confirmed by both theoretical deduction and numerical experiments. It has been reported that MAM is the season in which the most conspicuous difference is seen in the influences of EM and ENSO on Australia rainfall (Cai and Cowan 2009; Taschetto and England 2009), and it has been demonstrated that the influences of the two types of ENSO on south China rainfall during this season is opposite (Feng and Li 2011). The present results provide a plausible explanation for this phenomenon; that is, the meridional structure of SST anomalies associated with ENSO and EM are most different during MAM, which in turn may result in contrasting influences and teleconnections. This possibility is established by the relationships between meridional SST indices (MSSI and MASI) and global rainfall (figure not shown). It is seen that opposite influences of asymmetric and symmetric variations of tropical SST on rainfall parallels the anomalous pattern associated with EM and ENSO, respectively. This further suggests that the different influences of ENSO and EM on the regional climate are caused not only by the different positions of the warming centers but also by the different meridional structure of SSTA.

In addition, we find that ENSO corresponds to symmetric variations in tropical SST, whereas EM corresponds to asymmetric variations, resulting in equatorially symmetric and asymmetric meridional circulations

during the boreal spring, respectively. However, it appears that the structure of zonal-mean SSTA associated with ENSO and EM is similar in other seasons (Figs. 1, 2). Thus, it would be interesting to further examine why the zonal-mean SSTA that accompanies EM in the boreal spring is different from those in other seasons, considering that opposite meridional circulation anomalies are induced. Of note, EM events are more frequent and stronger in future climatic scenarios (Yeh et al. 2009; Kim and Yu 2012). Therefore, it can be concluded that the EM-induced anomalous HC would also be more common in the future climate. As reported, the Southern Hemisphere HC expansion trends are strong in the boreal spring (Fu et al. 2006; Seidel and Randel 2007); it would be interesting to investigate whether EM has contributed to this poleward expansion of HC during the past three decades. The linear correlation coefficient between EMI and the poleward edge is about 0.23, not significant at the 0.05 level, implying that the impacts of EM on the poleward expansion of HC during boreal spring are limited. In this way, is it possible that there are some nonlinear processes involved? This is still an unresolved question and needs further work. Moreover, note that, although the anomalous patterns during the warm and cold events are opposite in both types of ENSO, there are some differences that exist in their amplitude. We found that the anomalous meridional circulation associated with El Niño is larger than those with La Niña; in contrast, the anomalous meridional circulation associated with El Niño Modoki is smaller than those with La Niña Modoki (figure not shown). This asymmetry is also seen in the SST indices: that is, MSSI and MASI. The values of MSSI for El Niño and La Niña years are 1.87° and −1.10°C, respectively. The values of MASI for El Niño Modoki and La Niña Modoki years are 0.68° and −0.94°C, respectively.

Finally, the present study highlights the fact that EM and ENSO have opposite climatic influences on boreal spring HC. This finding underscores the importance of taking into account the influence of EM on HC. However, why the SSTA structure associated with EM in the boreal spring is different from SSTA structures in other seasons is still unknown. A recent study by Chiang and Vimont (2004) reported that there exists a meridional mode SSTA in the tropical Pacific (Fig. 1 in their work), which is independent of ENSO with the peak anomaly in the boreal spring. This mode is characterized by an anomalous displacement of the ITCZ toward the warmer hemisphere and is forced by trade wind variations in their respective northern subtropical oceans. This raises the possibility that the development of the meridional mode may contribute to the meridional SSTA pattern associated with EM, by which differences in the SSTA pattern between the spring and other seasons are induced. In this way, what is the relationship between the meridional mode and EM and underlying mechanisms? Furthermore, the impacts of ENSO on HC have been intensely explored, but other questions remain unanswered and warrant more work, including the following: 1) Does EM play a role in influencing HC in other seasons? 2) Does EM differ from ENSO in this regard? Given the observed fact that the relationship between ENSO and the East Asian summer monsoon (EASM) is enhanced within the past 50 yr (Li et al. 2010, 2011a,b), the weakening of EASM is associated with the weakening of boreal summer HC (Feng et al. 2011a). 3) What are the possible causes of these differences?

*Acknowledgments.* We thank three anonymous referees whose comments improved the paper. This work was jointly supported by the 973 Program (2010CB950400) and the National Natural Science Foundation of China (41205046 and 41030961).

## REFERENCES

Afzaal, M., J. Li, and F.-F. Jin, 2013: The asymmetric influence of the two types of El Niño and La Niña on summer rainfall over southeast China. *J. Climate,* **26,** 4567–4582.

Ashok, K., S. K. Behera, S. A. Rao, H. Weng, and T. Yamagata, 2007: El Niño Modoki and its possible teleconnection. *J. Geophys. Res.,* **112,** C11007, doi:10.1029/2006JC003798.

Bulic, I. H., and C. Brankovic, 2007: ENSO forcing of the Northern Hemisphere climate in a large ensemble of model simulation based on a very long SST record. *Climate Dyn.,* **28,** 231–254.

Cai, W., and T. Cowan, 2009: La Niña Modoki impacts Australia autumn rainfall variability. *Geophys. Res. Lett.,* **36,** L12805, doi:10.1029/2009GL037885.

Chang, E. K. M., 1995: The influence of Hadley circulation intensity changes on extratropical climate in an idealized model. *J. Atmos. Sci.,* **52,** 2006–2024.

Chao, J. P., and Z. G. Wang, 1991: Influence of the ocean heating scale on the structure of the vertical circulation cell in the tropical atmosphere. *J. Nanjing Inst. Meteor,* **14,** 10–17.

Chiang, J. C. H., and D. J. Vimont, 2004: Analogous Pacific and Atlantic meridional modes of tropical atmosphere–ocean variability. *J. Climate,* **17,** 4143–4158.

Collins, W. D., and Coauthors, 2006: The formulation and atmospheric simulation of the Community Atmosphere Model Version 3 (CAM3). *J. Climate,* **19,** 2144–2161.

Diaz, H. F., and B. Bradley, 2004: *The Hadley Circulation: Present, Past and Future.* Kluwer Academic, 511 pp.

Feng, J., and J. Li, 2011: Influence of El Niño Modoki on spring rainfall over South China. *J. Geophys. Res.,* **116,** D13102, doi:10.1029/2010JD015160.

——, ——, and H. L. Xu, 2012: Increased summer rainfall in northwest Australia linked to southern Indian Ocean climate variability. *J. Geophys. Res.,* doi:10.1029/2012JD018323.

——, ——, and F. Xie, 2013: Long-term variation of the principal mode of boreal spring Hadley circulation linked to SST over the Indo-Pacific warm pool. *J. Climate,* **26,** 532–544.

Feng, R., J. Li, and J. C. Wang, 2011a: The principal modes of variability of the boreal summer Hadley circulation and their variations (in Chinese). *Chin. J. Atmos. Sci.,* **35,** 201–206.

——, ——, and ——, 2011b: Regime change of the boreal summer Hadley circulation and its connection with the tropical SST. *J. Climate,* **24,** 3867–3877.

Fu, Q., C. M. Johanson, J. M. Wallace, and T. Reichler, 2006: Enhanced mid-latitude tropospheric warming in satellite measurements. *Science,* **312,** 1179.

Held, I. M., and A. Y. Hou, 1980: Nonlinear axially symmetric circulations in a nearly inviscid atmosphere. *J. Atmos. Res.,* **37,** 515–533.

Hou, A. Y., 1998: Hadley circulation as a modulator of the extratropical climate. *J. Atmos. Sci.,* **55,** 2437–2457.

——, and R. S. Lindzen, 1992: The influence of concentrated heating on the Hadley circulation. *J. Atmos. Sci.,* **49,** 1233–1241.

Kalnay, E., and Coauthors, 1996: The NCEP/NCAR 40-Year Reanalysis Project. *Bull. Amer. Meteor. Soc.,* **77,** 437–471.

Kao, H. Y., and J. Y. Yu, 2009: Contrasting eastern Pacific and central Pacific types of El Niño. *J. Climate,* **22,** 615–632.

Kaplan, A., M. A. Cane, Y. Kushnir, A. C. Clement, M. B. Blumenthal, and B. Rajagopalan, 1998: Analyses of global sea surface temperature 1856–1991. *J. Geophys. Res.,* **103,** 18 567–18 589.

Kim, S. T., and J.-Y. Yu, 2012: The two types of ENSO in CMIP5 models. *Geophys. Res. Lett.,* **39,** L11704, doi:10.1029/2012GL052006.

Kug, J.-S., F.-F. Jin, and S.-I. An, 2009: Two types of El Niño events: Cold tongue El Niño and warm pool El Niño. *J. Climate,* **22,** 1499–1515.

Larkin, N. K., and D. E. Harrison, 2005: On the definition of El Niño and associated seasonal average U.S. weather anomalies. *Geophys. Res. Lett.,* **32,** L13705, doi:10.1029/2005GL022738.

Lee, T., and M. J. McPhaden, 2010: Increasing intensity of El Niño in the central-equatorial Pacific. *Geophys. Res. Lett.,* **37,** L14603, doi:10.1029/2010GL044007.

Li, J., 2001: *Atlas of Climate of Global Atmospheric Circulation I. Climatological Mean State* (in Chinese). China Meteorological Press, 279 pp.

——, Z. Wu, Z. Jiang, and J. He, 2010: Can global warming strengthen the East Asian summer monsoon? *J. Climate,* **23,** 6696–6705.

——, and Coauthors, 2011a: *Ocean-Atmosphere Interaction over the Joining Area of Asia and Indian-Pacific Ocean and Its Impact on the Short-Term Climate Variation in China.* Vol. I, China Meteorological Press, 516 pp.

——, and Coauthors, 2011b: *Ocean-Atmosphere Interaction over the Joining Area of Asia and Indian-Pacific Ocean and Its Impact on the Short-Term Climate Variation in China.* Vol. II, China Meteorological Press, 565 pp.

——, J. Feng, and Y. Li, 2012: A possible cause of decreasing summer rainfall in northeast Australia. *Int. J. Climatol.,* **32,** 995–1005, doi:10.1002/joc.2328.

——, and Coauthors, 2013: Progress in air-land-sea interactions in Asia and their role in global and Asian climate change. *Chin. J. Atmos. Sci.,* **37,** 518–538.

Lindzen, R. S., 1994: Climate dynamics and global change. *Annu. Rev. Fluid Mech.,* **26,** 353–378.

——, and S. Nigam, 1987: On the role of sea surface temperature gradients in forcing low-level winds and convergence in the tropics. *J. Atmos. Sci.,* **44,** 2418–2436.

——, and A. Y. Hou, 1988: Hadley circulations for zonally averaged heating centered off the equator. *J. Atmos. Sci.,* **45,** 2416–2427.

Ma, J., and J. Li, 2007: The reason for the strengthening of the boreal winter Hadley circulation and its connection with ENSO. *Prog. Nat. Sci.,* **17,** 1327–1333.

——, and ——, 2008: The principal modes of variability of the boreal winter Hadley cell. *Geophys. Res. Lett.,* **35,** L01808, doi:10.1029/2007GL031883.

Mitas, C. M., and A. Clement, 2005: Has the Hadley cell been strengthening in recent decades? *Geophys. Res. Lett.,* **32,** L03809, doi:10.1029/2004GL021765.

Oort, A. H., and J. J. Yienger, 1996: Observed interannual variability in the Hadley circulation and its connection to ENSO. *J. Climate,* **9,** 2751–2767.

Quan, X. W., H. F. Diaz, and M. P. Hoerling, 2004: Changes of the tropical Hadley cell since 1950. *The Hadley Circulation: Present, Past and Future,* H. F. Diaz and R. S. Bradley, Eds., Springer, 85–120.

Rasmusson, E. M., and T. H. Carpenter, 1982: Variations in tropical sea surface temperature and surface wind fields associated with the Southern Oscillation/El Niño. *Mon. Wea. Rev.,* **110,** 354–384.

Rayner, N. A., D. E. Parker, E. B. Horton, C. K. Folland, L. V. Alexander, D. P. Rowell, E. C. Kent, and A. Kaplan, 2003: Global analyses of sea surface temperature, sea ice, and night marine air temperature since the late nineteenth century. *J. Geophys. Res.,* **108,** 4407, doi:10.1029/2002JD002670.

Ren, H.-L., and F.-F. Jin, 2011: Niño indices for two types of ENSO. *Geophys. Res. Lett.,* **38,** L04704, doi:10.1029/2010GL046031.

Seager, R., N. Harnik, Y. Kushnir, W. Robinson, and J. Miller, 2003: Mechanisms of hemispherically symmetric climate variability. *J. Climate,* **16,** 2960–2978.

Seidel, D. J., and R. J. Randel, 2007: Recent widening of the tropical belt: Evidence from tropopause observations. *J. Geophys. Res.,* **112,** D20113, doi:10.1029/2007JD008861.

Smith, T. M., and R. W. Reynolds, 2004: Improved extended reconstruction of SST (1854–1997). *J. Climate,* **17,** 2466–2477.

Stachnik, J. P., and C. Schumacher, 2011: A comparison of the Hadley circulation in modern reanalyses. *J. Geophys. Res.,* **116,** D22102, doi:10.1029/2011JD016677.

Tanaka, H. L., N. Ishizaki, and A. Kitoh, 2004: Trend and interannual variability of Walker, monsoon and Hadley circulations defined by velocity potential in the upper troposphere. *Tellus,* **56A,** 250–269.

Taschetto, A. S., and M. H. England, 2009: El Niño Modoki impacts on Australian rainfall. *J. Climate,* **22,** 3167–3174.

Trenberth, K. E., 1997: The definition of El Niño. *Bull. Amer. Meteor. Soc.,* **78,** 2771–2777.

——, and D. P. Stepaniak, 2001: Indices of El Niño evolution. *J. Climate,* **14,** 1697–1701.

Uppala, S. M., and Coauthors, 2005: The ERA-40 Re-Analysis. *Quart. J. Roy. Meteor. Soc.,* 131, 2961–3012.

Wang, C. Z., and R. H. Weisberg, 2000: The 1997–98 El Niño evolution relative to previous El Niño events. *J. Climate,* **13,** 488–501.

Weng, H. Y., K. Ashok, S. K. Behera, S. A. Rao, and T. Yamagata, 2007: Impacts of recent El Niño Modoki on dry/wet conditions in the Pacific Rim during boreal summer. *Climate Dyn.,* **29,** 123–129.

——, S. K. Behera, and T. Yamagata, 2009: Anomalous winter climate conditions in the Pacific Rim during recent El Niño Modoki and El Niño events. *Climate Dyn.,* **32,** 663–674.

Xie, F., J. Li, W. Tian, J. Feng, and Y. Huo, 2012: Signals of El Niño Modoki in the tropical tropopause layer and stratosphere. *Atmos. Chem. Phys.,* **12,** 5259–5273, doi:10.5194/acp-12-5259-2012.

Yeh, S.-W., J.-S. Kug, B. Dewitte, M.-H. Kwon, B. P. Kirtman, and F.-F. Jin, 2009: El Niño in a changing climate. *Nature,* **461,** 511–514, doi:10.1038/nature08316.

Yu, J. Y., and H. K. Kao, 2007: Decadal changes of ENSO persistence barrier in SST and ocean heat content indices: 1958–2001. *J. Geophys. Res.,* **112,** D13106, doi:10.1029/2006JD007654.

——, and S. T. Kim, 2010: Identification of central-Pacific and eastern-Pacific types of ENSO in CMIP3 models. *Geophys. Res. Lett.,* **37,** L15705, doi:10.1029/2010GL044082.

——, and ——, 2011: Relationships between extratropical sea level pressure variations and the central Pacific and eastern Pacific types of ENSO. *J. Climate,* **24,** 708–720.

Zhang, W., J. Li, and F.-F. Jin, 2009: Spatial and temporal features of ENSO meridional scales. *Geophys. Res. Lett.,* **36,** L15605, doi:10.1029/2009GL038672.

——, ——, and X. Zhao, 2010: The SST cooling mode in the Pacific cold tongue. *J. Geophys. Res.,* **115,** C12042, doi:10.1029/2010JC006501.

——, F.-F. Jin, J. Li, and H.-L. Ren, 2011: Contrasting impacts of two-type El Niño over the western North Pacific during boreal autumn. *J. Meteor. Soc. Japan,* **89,** 563–569.

——, ——, H.-L. Ren, J. Li, and J. X. Zhao, 2012: Differences in teleconnection over the North Pacific and rainfall shift over the USA associated with two types of El Niño during boreal autumn. *J. Meteor. Soc. Japan,* **90,** 535–552.

Zhao, Y., and J. Li, 2006: Discrepancy of mass transport between the Northern and the Southern Hemisphere among the ERA-40, NCEP/NCAR, NCEP-DOE AMIP-2, and JRA-25 reanalysis. *Geophys. Res. Lett.,* **33,** L20804, doi:10.1029/2006GL027287.